Journal of Electrical Engineering, Vol. 75, No. 1, 2024, pp. 56-62

sciendo

PAPERS

Experimental test performance for a comparative evaluation of a voltage source inverter: Dual voltage source inverter

Mrutyunjaya Mangaraj[1], Jogeswara Sabat[2], Ajit Kumar Barisal[2]

This article proposes an adaptive Kernel-Hebbian least mean square (KHLMS) controller for a dual voltage source inverter (VSI). The recommended topology consists of a distributed energy resource (DER) supported VSI called main VSI (MVSI) and split capacitor supported VSI termed as auxiliary VSI (AVSI). Both the MVSI and AVSI are used to serve the shunt compensation when DER is not integrated with MVSI. The DER scenario is considered to suppress the active power flow shortage in the utility grid. Here, optimal active power flow control (OAPFC) is managed by MVSI and shunt compensation is achieved by AVSI during DER operated mode. Hence, a dual VSI based distribution static compensator (DSTATCOM) facilitates the configuration merits such as reduction in system downtime cost, filter rating switching stress etc. Supremacy of both the neural network (NN) based controller and topology is presented by comparing VSI (called AVSI) in the context of harmonic reduction in source side, voltage balancing, power factor (PF) enhancement, better voltage regulation and OAPFC. The experimental results are obtained through field programmable gate array (FPGA) based hardware units which exhibit radical improvement in the power quality (PQ) conferring as per the international standard grid code (IEEE-519-2017).

Keywords: MVSI, AVSI, KHLMS, DSTATCOM, DER and PQ

1 Introduction

1.1 Motivation and incitement

Nowadays, the integration of DER with the utility grid has captured more attention due to the negative aspects of conventional resources and the traditional operation of the utility grid [1-3]. The conventional process of integrating the DER is the direct support to the utility or supplied into the grid [4-6]. In both cases, VSI along with power stage conversion is an important requirement. Conversely, the issues of the DER integration are the requirement of an extra power stage conversion and OAPFC management. Also, the high initial cost and seasonal power increase the cost efficiency of the DER integration system [7-9]. It is very important to deal with these challenges, to make the utility grid maximum efficient with economic benefits for consumers, has become necessary. To avoid the DER integration issues, power electronics devices that interface the non-conventional sources to the utility grid can be intended. It also realizes multiple operations, like, as reducing dependency on conventional sources, active power variation suppression and reducing PQ issues [10, 11].

1.2 Literature review

The conventional two-level VSI is used extensively among the commercially existing inverters due to its simple design and operation [12]. Also, it is found that the VSI has the marginal compensation capability due to the single pathway power supply. Besides these demerits some other negative aspects are also found such as buck converter [10, 13], high rating DC link voltage [14], unable to arrest circulating current [15], more switching stresses, high rating of filter inductance [16] and for DER integration the rating of the inverter will increase. At the beginning of the twentieth century, dual inverter topology underwent a fast evolution to replace the single VSI architecture, which includes flexibility, reduced total harmonic distortion (THD), lower EMI emission, less semiconductor device stress, high reliability, and arrest the zero-sequence current [13-16]. The superior features offered by dual VSI topology leads to a momentous penetration in areas like electric vehicles [17], PV system [18], electric drives [19], active power filters [14] and utility grid [10, 14, 15, 18]. Because of their inherent merits including source current shaping, unity PF, voltage balanced at the point of common coupling (PCC) and better voltage regulation are receiving much more and wider attention. This innovation has fully fledged to enhance the overall performance by providing a double current pathway [15]. The enhancement of source current shaping garnishes to the utility grids is observed in the past research work when the proposed topology i.e. dual VSI is utilized in grid operations [10, 14, 15].

[1]Department of Electrical and Electronics Engineering, SRM University-AP, Amaravati, Andhra Pradesh, India-522240
[2]Department of Electrical Engineering, Odisha University of Technology and Research, Bhubaneswar, Odisha, India-751029
mrutyunjaya.m@srmap.edu.in, jogesh.electrical@gmail.com and akbarisal@outr.ac.in

https://doi.org/10.2478/jee-2024-0008, Print (till 2015) ISSN 1335-3632, On-line ISSN 1339-309X

1.3 Contribution and paper organization

To overcome the negative aspects of conventional VSI, this paper designs a dual VSI for better OAPFC management with PQ improvement. The dual VSI consists of a DER-supported VSI called MVSI and a split capacitor-supported VSI termed AVSI. Both the VSI can be used to serve the shunt compensation. The DER scenario is considered to suppress the active power flow shortage in the utility grid. Here, OAPFC is managed by MVSI and shunt compensation is achieved by AVSI during DER operated mode. Hence, it facilitates the configuration merits such as reduction in system downtime cost, filter rating switching stress etc. Meanwhile, it suffers from some demerits, such as higher costs and complex switching signal generations. The dual operation of the proposed single system neglects the higher cost and for complex pulse generation a NN based control algorithm is utilized. Some control techniques based on neural network are Gradient descent back propagation [20], Quasi Newton back propagation [21], Least mean fourth based NN [22], Naïve back propagation [23], and KHLMS [24]. However, an accurately tuned KHLMS algorithm has better performance than the other algorithm [25]. This research work also like to point out the main objectives of the paper, which are been listed below:

- The proposed system can be one of the upcoming custom power devices with nonconventional energy integration with several benefits such as reduced dc-link voltage, continuous input current, reduction in filter inductance, lower source current THD, PF correction, lower switching stress, easy fault identification and repair.
- All time quality power supply to the clients of the utility grid is maintained with less dependency on conventional sources.
- Both inverters have the shunt compensation capability, if MVSI is shut down from the utility grid, still the shunt compensation of the grid is achieved using AVSI.
- Simple computation exhibits less error and accomplishes fast response on variable loading.

The structure of this research paper is organized as follows. First, the principle of MVSI and AVSI with theoretical capability is presented in Section 1. Section 2 presents the proposed system circuit configuration, principle of operation and novelties. Section 3 presents the computation process of switching signal generation using the KHLMS controller. Section 4 presents experimental results performance evaluations, and related discussions. Eventually, the proposed work is concluded in Section 5.

2 Brief background

2.1 Circuit description and operation

Figure 1 depicts a complete schematic diagram of dual VSI topology. There are three legs with two controlled IGBTs per each leg, forming the MVSI and AVSI. It is utilized for OAPFC in the utility grid by DER supported MVSI and shunt compensation by split capacitors supported AVSI. Two compensating impedances Z_c and Z'_c are connected between the utility grid and the front side of the inverter to inject currents. In this configuration AVSI is an earth point clamped inverter, the function of AVSI is to provide shunt compensation with arrested circulating current and unbalanced current. Two split capacitors are connected in series to form a common voltage DC link. A three-phase nonlinear and variable load drawing load current, and is connected at the PCC. Different nonconventional sources constitute the DER such as photovoltaic at variable low DC voltage, wind energy at variable AC voltage and fuel cell etc. So, these sources require power conditioning before connecting to the utility grid through MVSI. During experiments, a balanced three phase supply was connected through an autotransformer and isolation transformer to the rectifier, and the output of the rectifier was supplied to the MVSI. Here, a DC source is used in place of DER. The MVSI supplies the DER generated power into the three-phase utility grid.

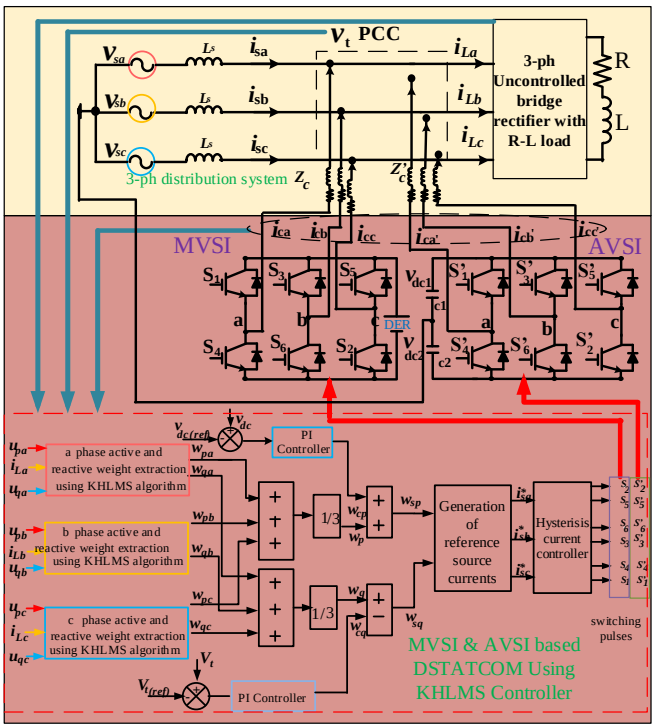

Fig. 1. Dual VSI topology with KHLMS controller

2.2 Novelties of the dual VSI based DSTATCOM

The dual VSI topology has improved characteristics with some novelties. The performances are highlighted below:

(i) *The components' breakdown rate reduced*: The dual VSI topology provides a two-way current path, i.e., load current divided by both MVSI and AVSI. If one fails then the other one can continue the operation. These factors increase the reliability and expiration time of components.
(ii) *Filter inductor rating reduced*: The rating of the VSI decreased which decreased the rating of the switch. But the switches switched at the higher switching frequency and the inductance of the filter is decreased.
(iii) *Round the clock power supply*: The MVSI is supported by DER, when the main source of the utility grid fails MVSI can inject active power. This helps to provide continuous power supply to the end user of the utility grid.
(iv) *Flexibility of the system increased*: MVSI and AVSI were supplied from separate DC sources. i.e., MVSI and AVSI can operate separately. Hence the system flexibility will be increased.
(v) *THD reduction*: It is found from the experimental results that the dual VSI keeps its supply current THD less than the VSI and also keeps less than the value recommended by the IEEE grid code.
(vi) *Decrease in inverter DC link voltage*: The MVSI is a self-capacitor supported topology and AVSI is split capacitor supported topology. Hence MVSI DC-link voltage is reduced to 38% over AVSI because MVSI does not supply the zero-sequence load current component.
(vii) *Reduces dependence on conventional sources*: It reduces the dependence on conventional sources because the MVSI is integrated with non-conventional sources and its maximum capacity is utilized as active power transfer.

3 KHLMS control algorithm

In this proposed KHLMS algorithm, the step size and convergence factor are represented by α and γ. The range of both α and γ must be within 0 and 1. The KHLMS algorithm is trained (where, $\alpha = 0.4$ and $\gamma = 0.2$) to obtain the stable and convergence characteristics. In particular, the training study is analysed for the unit PF operation, less harmonic distortion and suitable amplitude of source current. Hence, both the values are chosen as the most accepted values [24]. The computation process for different variables is presented below:

3.1 Computation of load current's active component

The weighting values of the active component of the load current (w_{pa}, w_{pb}, w_{pc}) are obtained using the KHLMS algorithm as follows [24]:

$$w_{pa}(n) = \\ = \alpha\gamma\{f(i_{la})^T + f(i_{la})^T f(i_{la}) w_{pa}(n-1)\} i_{la} u_{pc}(n) \\ + w_{pa}(n-1), \quad (1)$$

$$w_{pb}(n) = \\ = \alpha\gamma\{f(i_{lb})^T + f(i_{lb})^T f(i_{lb}) w_{pb}(n-1)\} i_{lb} u_{pc}(n) \\ + w_{pb}(n-1), \quad (2)$$

$$w_{pc}(n) = \\ = \alpha\gamma\{f(i_{lc})^T + f(i_{lc})^T f(i_{lc}) w_{pc}(n-1)\} i_{lc} u_{pc}(n) \\ + w_{pc}(n-1), \quad (3)$$

where $w_{pa}(n-1)$ is the vector in phase a, $f(i_{la})^T = (i_{la1}, i_{la2} \ldots\ldots i_{lan})^T$, and $i_{lan} = n^{th}$ is the eigen-value of the load current ≥ 0.

3.2 Computation of load current's reactive component

Similarly, the extraction of weighting values of the reactive component of load current w_{qa}, w_{qb}, w_{qc} are obtained using the KHLMS algorithm as follows:

$$w_{qa}(n) = \\ = \alpha\gamma\{f(i_{la})^T f(i_{la})^T f(i_{la}) w_{qa}(n-1)\} i_{la} u_{qa}(n) \\ + w_{qa}(n-1) \quad (4)$$

$$w_{qb}(n) = \\ = \alpha\gamma\{f(i_{lb})^T f(i_{lb})^T f(i_{lb}) w_{qb}(n-1)\} i_{lb} u_{qb}(n) \\ + w_{qb}(n-1) \quad (5)$$

$$w_{qc}(n) = \\ = \alpha\gamma\{f(i_{lc})^T f(i_{lc})^T f(i_{lc}) w_{qc}(n-1)\} i_{lc} u_{qc}(n) \\ + w_{qc}(n-1) \quad (6)$$

The w_a average weight of active component can be expressed as:

$$w_a = \frac{w_{pa} + w_{pb} + w_{pc}}{3}. \quad (7)$$

The w_r average weight of reactive component can be expressed as:

$$w_r = \frac{w_{qa} + w_{qb} + w_{qc}}{3}. \quad (8)$$

3.3 Computation of unit voltage template

Here, v_t is termed as amplitude of PCC voltage and v_{sa} is the phase voltage. Therefore, for estimating unit voltage templates (u_{pa}, u_{pb}, u_{pc}), the phase voltage divided by the amplitude of PCC voltage is determined as

$$u_{pa} = \frac{v_{sa}}{v_t},\ u_{pb} = \frac{v_{sb}}{v_t},\ u_{pc} = \frac{v_{sc}}{v_t}. \quad (9)$$

The quadrature unit voltage templates (u_{qa}, u_{qb}, u_{qc}) is determined as

$$u_{qa} = \frac{u_{pb} + u_{pc}}{\sqrt{3}},\ \ u_{qb} = \frac{3u_{pa} + u_{pb} - u_{pc}}{2\sqrt{3}},$$
$$u_{qc} = \frac{-3u_{pa} + u_{pb} - u_{pc}}{2\sqrt{3}}, \quad (10)$$

where v_t can be stated as

$$v_t = \sqrt{\frac{2(v_{sa}^2 + v_{sb}^2 + v_{sc}^2)}{3}}. \quad (11)$$

3.4 Computation of source current's active component

The estimating error dc voltage v_{de} is determined as

$$v_{de} = v_{dc\,(ref)} - v_{dc}, \quad (12)$$

where $v_{dc\,(ref)}$ is the reference DC voltage and v_{dc} is the sensed DC voltage.

Based on the above analysis, the difference is processed through the Proportional-Integral controller. we can deduce the output as

$$w_{cp} = k_{pa} v_{de} + k_{ia} \int v_{de} dt. \quad (13)$$

The estimating the reference source current total active components is determined as

$$w_{sp} = w_a + w_{cp}, \quad (14)$$

where w_a is the average magnitude of the load currents active component and w_{cp} is the PI controller output.

3.5 Computation of source current's reactive component

The ac voltage error (v_{te}) is determined as

$$v_{te} = v_{t\,(ref)} - v_t. \quad (15)$$

Based on the above analysis, the difference is processed through the Proportional-Integral controller. we can deduce the output as

$$w_{cq} = k_{pr} v_{te} + k_{ir} \int v_{te} dt. \quad (16)$$

Here, w_r is termed as average magnitude of the load currents reactive component and w_{cq} is the PI controller output. Therefore, for estimating the reference source current total reactive components is determined as

$$w_{sq} = w_r - w_{cq}. \quad (17)$$

3.6 Generation of switching signal

The procedure of obtaining active part of instantaneous three-phase reference source side current is determined as

$$i_{aa} = w_{sp} u_{pa},\ \ i_{ab} = w_{sp} u_{pb},\ \ i_{ac} = w_{sp} u_{pc}. \quad (18)$$

The procedure of obtaining reactive part of instantaneous three-phase reference source side current can deduce as

$$i_{ra} = w_{sq} u_{qa},\ \ i_{rb} = w_{sq} u_{qb},\ \ i_{rc} = w_{sq} u_{qc}. \quad (19)$$

Therefore, for estimating the reference source current can deduce as follows:

$$i_{sa}^* = i_{aa} + i_{ra}, i_{sb}^* = i_{ab} + i_{rb}, i_{sc}^* = i_{ac} + i_{rc}. \quad (20)$$

Here, i_{sa}, i_{sb}, i_{sc} are termed as actual source currents and i_{sa}^*, i_{sb}^*, i_{sc}^* are the source currents (reference). Therefore, for generating the error signals both are compared. Afterward, the error is precise to a Hysteresis Current Controller (HCC). The outputs of HCC are used to supply the pulses of switches S_1 to S_6 of the AVSI and S'_1 to S'_6 of the MVSI.

4 Hardware implementation and results

The merits of the proposed topology are designed and verified through experimentation. The hardware unit seen in Fig. 2 is constructed using system parameters as those arranged in Tab. 1. The SPARTAN-6 FPGA controller switching frequency is 20 kHz, which operates the switches of MVSI and AVSI. The KHLMS control algorithm is designed in XILINX SP6 LX25 and coded for implementation in the FPGA controller toolbox. The sampling rate is kept to 50 μs to avoid overrun errors. The voltage, current, PF and harmonic reduction are recorded with 200 ms averages by using a digital storage oscilloscope (model no-SIGLENT, SDS1104X-E-5100) and multifunction meter (MFM) model no-SELEC-MFM384, which is fully compatible with IEC-614000-4-30.

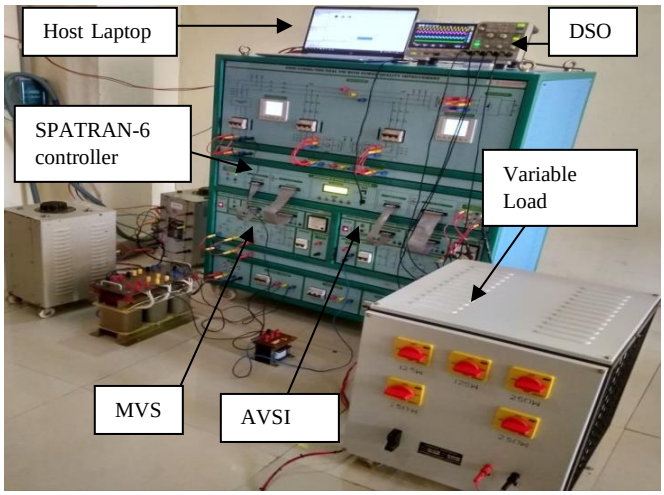

Fig. 2. Experimental unit of the proposed topology

A 3-phase variable nonlinear load, i.e., a diode bridge rectifier with variable *R* and fixed *L* is supplied by MVSI and AVSI topology. Two MFMs are connected at source side MFM-1 and load side MFM-2 of the utility grid to measure different parameters such as voltage, current, power, PF and THD of the system.

4.1 Operational performance of conventional VSI

The experimental waveform of the source voltage and three phase source currents with and without VSI are depicted in Fig. 3(a) it is found that no distortions are present in the source currents after compensation. Figure 3(b) shows the distortion present in the source current before VSI switched ON. The a-phase source current and voltage are in phase and sinusoidal when VSI based DSTATCOM is switched ON. Figures 3(c-d) show the THD reduction and PF correction after compensation.

4.2 Superior performance of proposed topology

The MVSI and AVSI are connected at the PCC of the utility grid, the switches of AVSI are first switched on and the performance is similar to the two-level VSI. But when dual VSI is switched on, the performance of the system is improved and its results in phase *a* source voltage and three phase source currents are shown in Fig. 4(a). The inherent merits of the proposed configuration are that it decreases the DC link voltage of MVSI up to 38% over AVSI and is stable at 570 V and the total DC link voltage across two split capacitors of AVSI is 904 V. The proposed dual VSI exhibits admirable dynamic performance, phase-a source voltage, phase-a source currents, phase-a compensating current of AVSI and phase-a compensating current of MVSI are shown in Fig. 4(b).

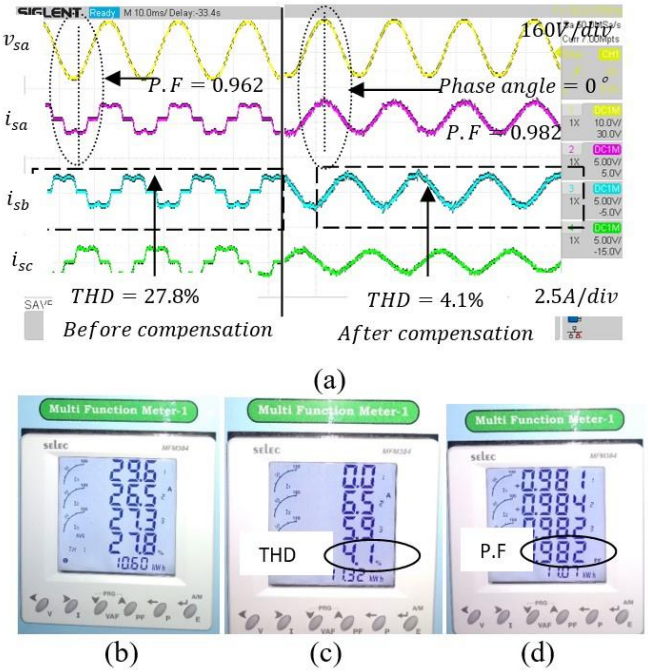

Fig. 3. Performance of VSI, (a) v_{sa} (phase *a* supply voltage) and i_{sa}, i_{sb}, i_{sc} (3-phase supply current) before and after compensation, (b) distortion in source currents before compensation, (c) distortion free source currents after compensation and (d) after compensation PF improvement

It is observed from Fig. 4(c), that after compensation, the three phase source currents THDs are reduced to (average) 2.4% and the PF corrected to 0.985 is shown in Fig. 4(d). The experimental outcome of dual VSI compared with conventional VSI and the dynamic performance of the KHLMS technique with others are arranged in Tab. 2 and Tab. 3 respectively.

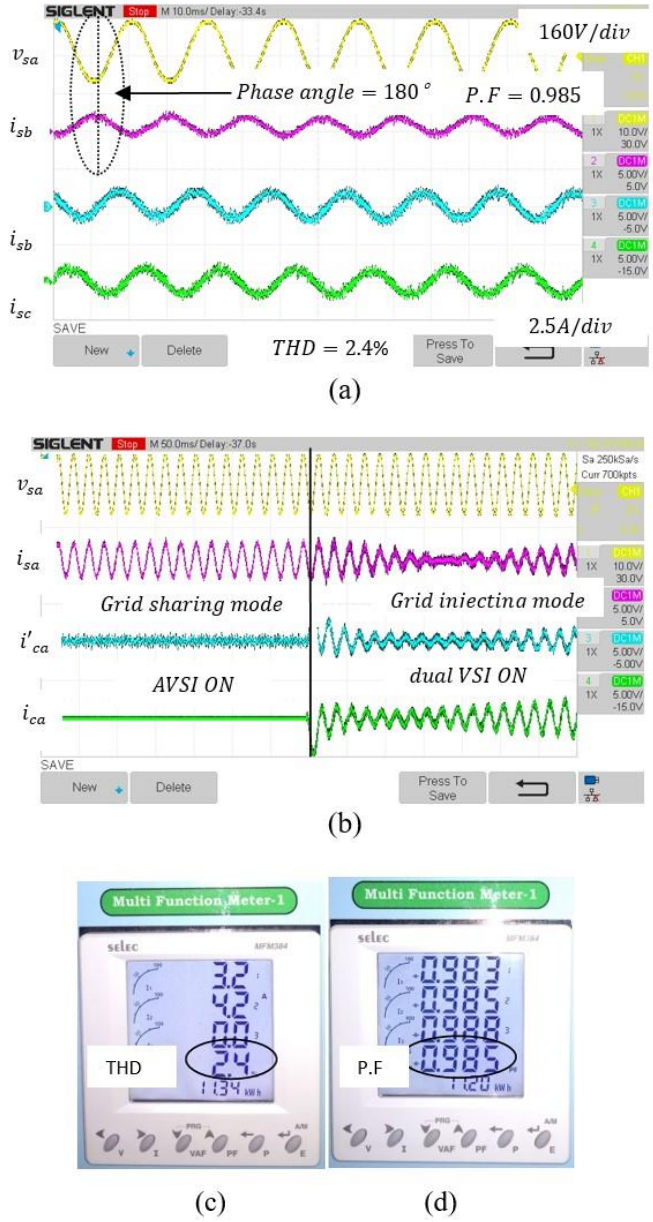

Fig. 4. Superior performance of the dual VSI: (a) v_{sa} (phase a supply voltage) and i_{sa}, i_{sb}, i_{sc} (3-phase supply current) before and after compensation, (b) phase a supply voltage, supply current, compensating current of AVSI and MVSI, (c) distortion free source currents after compensation, and (d) after compensation PF improvement

Table 1. Hardware unit parameters and magnitude

Required parameter	Magnitude
Source voltage	200 V/phase
Microgrid voltage	415 V (line to line)
System frequency	50 Hz
Switching frequency	20 kHz
Source resistance	5 Ω
Variable load	1 kW
Compensator resistance	50 Ω
Compensator inductance	5 mH
Inverter rating	2 kVA, 5 A
DC link voltage	750 V(max)
DC link capacitor	2200 µF
Isolation Transformer	3 kVA, 415 V
Variable Transformer (No 2)	5 kVA, (0-470 V)

Table 2. Assessment of single VSI and dual VSI

Parameter	VSI	dual VSI
i_s (A), %THD	2.3, 4.1	2.1, 2.4
v_s (V), %THD	200, 1.6	202, 1.4
i_l (A), %THD	1.8, 29	1.83, 29
PF	0.982	0.985
Active power injection	NO	Yes
DC link voltage (V)	904 V	904 V(AVSI) 570 V(MVSI)

Table 3. Assessment between other techniques for source current harmonics reduction with the KHLMS

Measurement	Source current THD%	Load current THD%	PF
Ref. [14]	4.14	27.9	0.9
Ref. [25]	3.8	27.9	0.8
KHLMS technique	2.4	29	0.98

5 Conclusion

The reliability, flexibility and shunt compensation capability of the inverter is improved, which can also regulate the OAPFC. Some important contributions of the dual VSI are highlighted below:

- Auxiliary power supply requirement is omitted when the source side fails in the utility grid.
- More reliable and the overall performance is better over single VSI.
- Modularity is possible, future upcoming noncon-ventional sources can be integrated with the proposed topology.
- Fault identification and maintenance is easy and can be done without a whole system shutdown.
- The switching losses are reduced due to the dual current path way.
- Reduced THD of source currents, better voltage regulation with balanced voltage at PCC and under variable nonlinear loading maintaining source PF nearer to unity and sinusoidal.

Validation of the proposed topology under variable nonlinear conditions is verified with the experimental setup. Finally, the proposed topology found a more suitable option for a low and medium voltage utility grid.

Acknowledgment

We acknowledge the support of the Science and Engineering Research Board of India (SERB-DST), Sanction number: SERB/F/8504/2019-2020.

References

[1] J. Sabat, M. Mangaraj, "Operation and Control Performance of Interactive DZSI-Based DSTATCOM," *J. Inst. Eng. India Ser. B*, 2022. https://doi.org/10.1007/s40031-022-00730-w

[2] M. Shaheen, R. A. El-Sehiemy, S. Kamel, E. E. Elattar and A. M. Elsayed, "Improving Distribution Networks' Consistency by Optimal Distribution System Reconfiguration and Distributed Generations," *IEEE Access*, vol. 9, pp. 67186-67200, 2021, doi: 10.1109/ACCESS.2021.3076670.

[3] G. D. Marques, M. F. Iacchetti and S. M. A. Cruz, "An Explicit Minimum-Loss Control Strategy for Dual VSI DFIG-DC Systems," *IEEE Journal of Emerging and Selected Topics in Power Electronics*, vol. 11, no. 5, pp. 5234-5243, Oct. 2023, doi: 10.1109/JESTPE.2023.3289504.

[4] M. K. Kar, A. K. Singh, S. Kumar et al. "Application of Fractional-Order PID Controller to Improve Stability of a Single-Machine Infinite-Bus System," *J. Inst. Eng. India Ser. B* , 2023. https://doi.org/10.1007/s40031-023-00950-8

[5] M. K. Kar, B. Rout and J. K. Moharana, "Improvement of power factor of a grid connected load system using a static compensator," *Journal for Foundations and Applications of Physics*, vol. 1, no. 1, pp.5-10, 2014.

[6] D. A. Patel, K. Venkatraman, V. R. R. Rudra Raju, et al. "A Dual Functional DSTATCOM for Power Quality Improvement," *J. Inst. Eng. India Ser. B*, vol. 102, pp. 881–893, 202, https://doi.org/10.1007/s40031-021-00575-9

[7] A. Akhavan, J. C. Vasquez and J. M. Guerrero, "A Robust Method for Controlling Grid-Connected Inverters in Weak Grids," *IEEE Transactions on Circuits and Systems II: Express Briefs*, vol. 68, no. 4, pp.1333-1337, 2021, doi: 10.1109/TCSII.2020.3033427

[8] M. K. Kar, S. Kumar, A. K. Singh, "Power Quality Improvement of an Interconnected Grid System Using PWM Technique of D-STATCOM," In: Kumar, S., Singh, B., Singh, A.K. (eds) Recent Advances in Power Electronics and Drives. *Lecture Notes in Electrical Engineering*, vol. 852, 2022. Springer, Singapore. https://doi.org/10.1007/978-981-16-9239-0_3

[9] P. Zhao, et al, "Economic-Effective Multi-Energy Management Considering Voltage Regulation Networked with Energy Hubs," *IEEE Transactions on Power Systems*, vol. 36, no. 3, pp. 2503-2515, 2021, doi: 10.1109/TPWRS.2020.3025861

[10] M. K. Kar, "Stability analysis of multi-machine system using FACTS devices," *Int J Syst Assur Eng Manag*, vol. 14, pp. 2136–2145, 2023. https://doi.org/10.1007/s13198-023-02044-6

[11] M. V. Manoj Kumar, M. K. Mishra and C. Kumar, "A Grid-Connected Dual Voltage Source Inverter with Power Quality Improvement Features," *IEEE Transactions on Sustainable Energy*, vol. 6, no. 2, pp. 482-490, 2015.

[12] B. Singh, P. Jayaprakash, D. P., Kothari, A. Chandra and K. A. Haddad, "Comprehensive Study of DSTATCOM Configurations," *IEEE Transactions on Industrial Informatics*, vol. 10, no. 2, pp. 854-870, 2014.

[13] N. Rana, S. Banerjee, S. K. Giri, A. Trivedi and S. S. Williamson, "Modeling, Analysis and Implementation of an Improved Interleaved Buck-Boost Converter," *IEEE Transactions on Circuits and Systems II: Express Briefs*, vol. 68, no. 7, pp. 2588-2592, 2021, doi: 10.1109/TCSII.2021.3056478.

[14] M. Mangaraj, and J. Sabat, "MVSI and AVSI-supported DSTATCOM for PQ Analysis," *IETE Journal of Research*, vol. 69, no. 6, pp. 3852-3858, 2023, DOI: 10.1080/03772063.2021.1920850

[15] A. Aghazadeh, M. Davari, H. Nafisi, and F. Blaabjerg, "Grid Integration of a Dual Two-Level Voltage-Source Inverter Considering Grid Impedance and Phase-Locked Loop," *IEEE Journal of Emerging and Selected Topics in Power Electronics*, vol. 9, no. 1, pp. 401-422, 2021.

[16] Z. Ji, Q. Wang, D. Li, and Y. Sun, "Fast DC-Bias Current Control of Dual Active Bridge Converters with Feedforward Compensation*," IEEE Transactions on Circuits and Systems II: Express Briefs*, vol. 67, no. 11, pp. 2587-2591, 2020, doi: 10.1109/TCSII.2019.2957790.

[17] H. V. Nguyen, D. To, and D. Lee, "Onboard Battery Chargers for Plug-in Electric Vehicles with Dual Functional Circuit for Low-Voltage Battery Charging and Active Power Decoupling," *IEEE Access*, vol. 6, pp. 70212-70222, 2018, doi: 10.1109/ACCESS.2018.2876645.

[18] N. Kumar, T. K. Saha, and J. Dey, "Sliding-mode control of PWM dual inverter-based grid-connected PV system: Modeling and performance analysis, *IEEE Journal of Emerging and Selected Topics in Power Electronics*, vol. 4, no. 2, pp. 435-444, 2016.

[19] K. R. Sekhar, and S. Srinivas, "Discontinuous decoupled PWMs for reduced current ripple in a dual two-level inverter fed open-end winding induction motor drive," *IEEE Transactions on Power electronics*, vol. 28, pp. 2493-2502, 2013.

[20] M. Mangaraj and A. K. Panda, "Performance analysis of DSTATCOM employing various control algorithms," *IET Generation, Transmission and Distribution*, vol. 11, no. 10, pp. 2643-2653, 2017.

[21] A.K. Panda and M. Mangaraj, "DSTATCOM employing hybrid neural network control technique for power quality improvement," *IET Power Electronics*, vol. 10, no. 4, pp. 480-489, 2017.

[22] R. K. Agarwal, I. Hussain and B. Singh, "Application of LMS-Based NN Structure for Power Quality Enhancement in a Distribution Network Under Abnormal Conditions," *IEEE Transactions on Neural Networks and Learning Systems*. vol. 29, no. 5, pp. 1598-1607, 2018.

[23] M. Mangaraj and A. K. Panda, "NBP-based icosϕ control strategy for DSTATCOM," *IET Power Electronics*, vol. 10, no. 12, pp. 1617-1625, 2017.

[24] M. Mangaraj and A. K. Panda, "Modelling and simulation of KHLMS algorithm-based DSTATCOM," *IET Power Electronics*, vol. 12, no. 9, pp. 2304-2311, 2019.

[25] D. Vijay M., B. Singh, and G. Bhuvaneswari, "A High-Performance Microgrid with a Mechanical Sensorless SynRG Operated Wind Energy Generating System," *IEEE Transactions on Industrial Informatics*, vol. 16, no. 12, pp. 7349-7359, 2020.

Received 23 December 2023